"Schizophrenic" Micellization Associated with Coil-to-Helix Transitions Based on Polypeptide Hybrid Double Hydrophilic Rod–Coil Diblock Copolymer

Jingyi Rao, Zhaofeng Luo, Zhishen Ge, Hao Liu, and Shiyong Liu*

Department of Polymer Science and Engineering, Joint Laboratory of Polymer Thin Films and Solution, Hefei National Laboratory for Physical Sciences at the Microscale, University of Science and Technology of China, Hefei, Anhui Province 230026, China

Received July 29, 2007; Revised Manuscript Received September 19, 2007

A polypeptide hybrid double hydrophilic diblock copolymer (DHBC), poly(*N*-isopropylacrylamide)-*b*-poly(L-glutamic acid) (PNIPAM-*b*-PLGA), was synthesized via the ring-opening polymerization of γ-benzyl-L-glutamate *N*-carboxyanhydride (BLG-NCA) using monoamino-terminated PNIPAM as the macroinitiator, followed by deprotection of benzyl groups under alkaline conditions. Containing a thermoresponsive PNIPAM block and a pH-responsive PLGA block, the obtained polypeptide hybrid diblock copolymer molecularly dissolves in aqueous solution at alkaline pH and room temperature but supramolecularly self-assembles into PNIPAM–core micelles at alkaline pH and elevated temperatures and PLGA–core micelles at acidic pH and room temperature accompanied with coil-to-helix transition of the PLGA sequence. The pH- and thermoresponsive "schizophrenic" micellization behavior of PNIPAM-*b*-PLGA diblock copolymer has been investigated by ^{1}H NMR, optical transmittance, fluorescence probe measurement, transmission electron microscopy (TEM), dynamic and static laser light scattering (LLS), and circular dichroism (CD) spectroscopy. Moreover, the micellization process was investigated employing stopped-flow light scattering technique. The pH-induced micelle growth of PNIPAM-*b*-PLGA in aqueous solution exhibits drastically different kinetics compared to that of conventional pH-responsive DHBCs, probably due to the stabilization effects exerted by the formed α-helix secondary structures within the PLGA core at low pH. Exhibiting "schizophrenic" micellization, the polypeptide sequence of PNIPAM-*b*-PLGA can either locate within micelle cores or stabilizing coronas. The incorporation of polypeptide block into DHBCs can endow them with structural versatility, tunable spatial arrangement of chain segments within self-assembled nanostructures, and broader applications in the field of biomedicines.

Introduction

In selective solvents, block copolymers can self-assemble into mesophases with a variety of morphologies, such as micelles, vesicles, tubules, and complex superaggregates, depending on the relative block lengths, solvent compositions, concentrations, external additives, and temperature, etc.[1–8] Among them, polypeptide hybrid block copolymers consisting of synthetic polymer blocks and polypeptide segments represent a special type.[9–12] The presence of peptide segment endows the diblock copolymer with more complex and intriguing supramolecular nanostructures through hierarchical self-assembly in bulk and in solution, partially due to the formation of a characteristic protein-folding motif via inter- and intramolecular interactions. Molecular structure of the polypeptide hybrid block can be tailor-made via the *N*-carboxyanhydride (NCA) ring-opening polymerization (ROP) technique; moreover, they are generally nontoxic, biodegradable, and can be further functionalized due to the presence of reactive carboxyl and amino groups.[9,10,13–15]

A large amount of literature has documented the supramolecular self-assembly of peptide hybrid block copolymers in aqueous solution. They can be further categorized into two main types. The first one involves nanostructures with corona-forming polypeptide segments, starting from hybrid block copolymers consisting of hydrophobic polybutadiene (PB) or polystyrene (PS) and hydrophilic poly(L-glutamic acid) (PLGA) or poly(L-lysine) (PLL) blocks. For instance, Lecommandoux, Klok, and their co-workers[13,16–21] reported the self-assembly of a series of PB-*b*-PLGA and PS-*b*-PLL diblock copolymers in aqueous media. The second type typically involves a water-insoluble polypeptide sequence as one of the building blocks. Cho et al.[22,23] studied the solution and bulk properties of poly(ϵ-benzyloxycarbonyl-L-lysine)-*b*-poly(ethylene glycol)-*b*-poly(ϵ-benzyloxycarbonyl-L-lysine) (PZLL-*b*-PEG-*b*-PZLL) hybrid triblock copolymers. They also synthesized thermosensitive polypeptide hybrid block copolymer, poly(*N*-isopropylacrylamide)-*b*-poly(γ-benzyl-L-glutamate) (PNIPAM-*b*-PBLG), which can self-assemble in aqueous solution into polymeric micelles consisting of hydrophobic PBLG cores and well-solvated PNIPAM coronas.[24–26]

Our recent research interests partially involve double hydrophilic block copolymers (DHBCs).[27–29] Subjected to physical or chemical transformations in aqueous solution, one of the blocks of DHBCs can be selectively rendered water insoluble while the other block still remains hydrophilic to stabilize the self-assembled aggregates. Moreover, certain DHBCs exhibit "schizophrenic" micellization properties, forming two or more types of aggregates with "invertible" nanostructures upon judicious adjustment of external conditions.[30–38]

PLGA or PLL chains can reversibly change their conformations, such as α-helix, β-sheet, and random coil under proper external stimuli such as pH, ionic strength, and temperature.[31,39–47] These conformational changes of polypeptides concomitantly result in changes of their water solubility. Recently, Schlaad et

* To whom correspondence should be addressed. E-mail: sliu@ustc.edu.cn.

10.1021/bm700830b CCC: $37.00
Published on Web 11/03/2007

Scheme 1. Schematic Illustration of the Synthesis of Polypeptide Hybrid Double Hydrophilic Diblock Copolymer, $PNIPAM_{65}$-*b*-$PLGA_{110}$

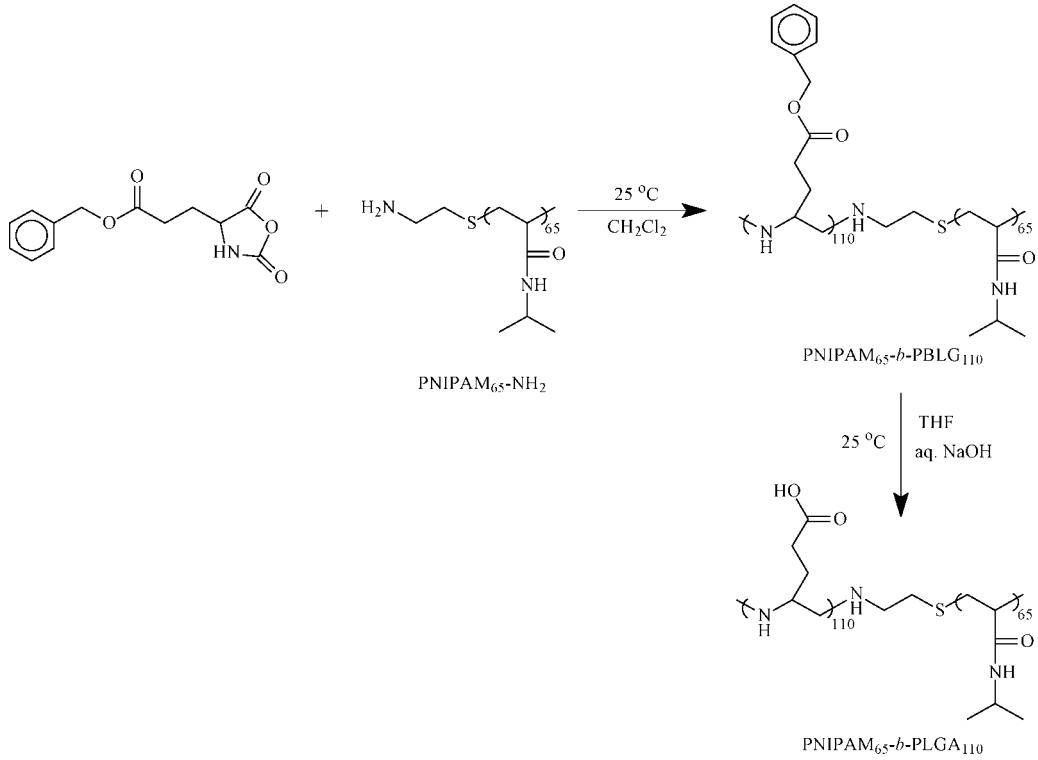

al.[48] described the synthesis of poly(2-isopropyl-2-oxazoline)-*b*-poly(L-glutamate) (PiPrOx-*b*-PLGA), using amino-terminated PiPrOx as the initiator for the ROP of NCA. However, the macroinitiator contains tertiary amine residues, which are also capable of initiating NCA polymerization via a different mechanism from that by primary amines. This might result in structural uncertainties for the target hybrid polypeptide diblock copolymers. Moreover, the self-assembly properties of PiPrOx-*b*-PLGA in aqueous media were not provided. It should be noted that, just recently, Lecommandoux et al.[49] reported the facile synthesis of a well-defined polypeptide hybrid diblock copolymer containing tertiary amine residues based on click chemistry.

To the best of our knowledge, "schizophrenic" micellization behavior of well-defined polypeptide hybrid DHBCs has not been reported yet. PNIPAM has been well-known as a thermoresponsive polymer, exhibiting a lower critical solution temperature (LCST) at ~32 °C.[50] Herein, we synthesized a novel polypeptide hybrid DHBC, PNIPAM-*b*-PLGA, via the ROP of γ-benzyl-L-glutamate *N*-carboxyanhydride (BLG-NCA) using monoamino-terminated PNIPAM as the macroinitiator, followed by deprotection of benzyl groups. The pH- and thermoresponsive "schizophrenic" micellization properties of PNIPAM-*b*-PLGA associated with coil-to-helix transitions were thoroughly investigated by ^{1}H NMR, optical transmittance, fluorescence measurement, laser light scattering (LLS), and circular dichroism (CD) spectroscopy. Moreover, the pH-induced micellization kinetics was also investigated by employing the stopped-flow light scattering technique, and the stabilization effects of α-helix formation within PLGA cores on the micellization processes were discussed.

Experimental Section

Materials. *N*-Isopropylacrylamide (NIPAM, 97%, Tokyo Kasei Kagyo Co.) was purified by recrystallization from a mixture of benzene and *n*-hexane (1/3, v/v). γ-Benzyl-L-glutamate (BLG) was prepared according to literature procedures.[51] 2,2′-Azobisisobutyronitrile (AIBN) was recrystallized from 95% ethanol. 2-Aminoethanethiol hydrochloride (AET·HCl) was purchased from Aldrich and used without further purification. Tetrahydrofuran (THF) and petroleum ether were dried by refluxing over sodium/benzophenone and distilled just prior to use. CH_2Cl_2 was distilled from CaH_2 under reduced pressure and subsequently stored over molecular sieves (4 Å) under an argon atmosphere. Trifluoroacetic acid (TFA) and all other chemicals were purchased from Shanghai Chemical Reagent Co. and used as received.

Monoamino-terminated PNIPAM, PNIPAM-NH_2, was synthesized by the free radical polymerization of NIPAM in methanol at 60 °C using AIBN and AET·HCl as initiator and chain transfer reagent, respectively.[52–54] The crude polydisperse amino-terminated PNIPAM was dissolved in water and further purified by consecutive dialysis using semipermeable membranes with cutoff molar masses of 7000 and 14000 g/mol, respectively. Amino-terminated PNIPAM fraction with molar mass within this range was then collected and freeze–dried. GPC analysis (Figure S1, Supporting Information) revealed that the purified amino-terminated PNIPAM sample possessed a number-average molecular weight, M_n, of 7400 (the degree of polymerization, DP = 65) and a polydispersity, M_w/M_n, of 1.31, it was denoted as $PNIPAM_{65}$-NH_2.[29]

Sample Preparation. The target diblock copolymer, PNIPAM-*b*-PLGA, was synthesized via the ROP of γ-benzyl-L-glutamate *N*-carboxyanhydride (BLG-NCA) using $PNIPAM_{65}$-NH_2 as the macroinitiator, followed by deprotection of the benzyl groups of PNIPAM-*b*-PBLG (Scheme 1). Detailed procedures for the preparation of BLG-NCA, $PNIPAM_{65}$-*b*-$PBLG_{110}$, and $PNIPAM_{65}$-*b*-$PLGA_{110}$ were described in Supporting Information. $PNIPAM_{65}$-*b*-$PLGA_{110}$ is directly soluble in alkaline media. The solution pH was adjusted by the addition of concentrated NaOH or HCl solutions.

Characterization. Molecular weights and molecular weight distributions were determined by gel permeation chromatography (GPC) using a series of two linear Styragel columns, HT3, HT4, and a column temperature of 35 °C. A Waters 1515 pump and a Waters 2414 differential refractive index detector (set at 30 °C) were used. The eluent was THF at a flow rate of 1.0 mL/min. A series of six low polydisperse

Scheme 2. Schematic Illustration of the Thermo- and pH-Responsive Micellization of PNIPAM$_{65}$-*b*-PLGA$_{110}$ associated with coil-to-helix transitions

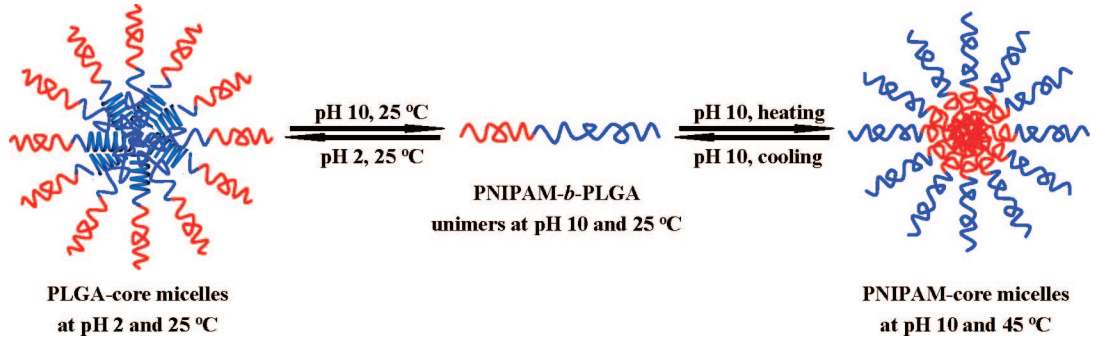

polystyrene standards with molecular weights ranging from 800 to 400000 g/mol were used for the GPC calibration. All ^{1}H NMR spectra were recorded in D_2O or $CDCl_3$ using a Bruker 300 MHz spectrometer. The optical transmittance of the solution was acquired on a Unico UV–vis 2802PCS spectrophotometer and measured at a wavelength of 600 nm using a thermostatically controlled cuvette. Fourier transform infrared (FT-IR) spectra were recorded on a Bruker VECTOR-22 IR spectrometer. The spectra were collected over 64 scans with a spectral resolution of 4 cm^{-1}. Circular dichroism (CD) spectra were recorded at 25 °C with a Jasco J-720 (Tokyo, Japan) spectrophotometer.

Fluorescence Spectroscopy. Fluorescence spectra were recorded using a Shimadzu RF-5301PC spectrofluorometer. The temperature of the water-jacketed cell holder was controlled by a programmable circulation bath. The slit widths were set at 5.0 nm for both the excitation and emission. Calculated volumes of pyrene solution in acetone was added into a series of volumetric flasks, acetone was removed under reduced pressure, polymer solutions at a concentration of 0.5 wt % were then added into volumetric flasks, and pyrene concentration was fixed at 5×10^{-7} mol/L. All the samples were sonicated for 2 h and then allowed to stand overnight before fluorescence measurements.

Laser Light Scattering (LLS). A commercial spectrometer (ALV/DLS/SLS-5022F) equipped with a multitau digital time correlator (ALV5000) and a cylindrical 22 mW UNIPHASE He–Ne laser (λ_0 = 632 nm) as the light source was employed for dynamic and static laser light scattering (LLS) measurements. In dynamic LLS, scattered light was collected for duration of ~10 min for each measurement at a fixed angle. The temperature was controlled by a programmable circulation bath. Each data point was obtained after the measured value was stable, which typically took ~0.5 h. Distribution averages and particle size distributions were computed using cumulants analysis and CONTIN routines. All data points were averaged over three measurements.

In static LLS, we can obtain the weight-average molar mass (M_w) and the *z*-average root-mean-square radius of gyration ($\langle R_g^2\rangle^{1/2}$ or written as $\langle R_g\rangle$) of polymer chains or aggregates in a dilute solution from the angular dependence of the excess absolute scattering intensity, known as Rayleigh ratio $R_{vv}(q)$, as

$$\frac{KC}{R_{vv}(q)} \approx \frac{1}{M_w}(1 + \frac{1}{3}\langle R_g\rangle q^2) + 2A_2C \qquad (1)$$

where $K = 4\pi^2 n^2 (dn/dC)^2/(N_A\lambda_0^4)$ and $q = (4\pi n/\lambda_0)\sin(\theta/2)$ with N_A, dn/dC, n, and λ_0 being the Avogadro number, the specific refractive index increment, the solvent refractive index, and the wavelength of the laser light in a vacuum, respectively, and A_2 is the second virial coefficient. The specific refractive index increment was determined by a precise differential refractometer. It should be noted that the obtained M_w values should be considered as apparent ones (denoted as $M_{w,app}$), as static LLS measurement was conducted for only one polymer concentration (0.05 g/L) and no extrapolation to zero concentration was conducted.

Transmission Electron Microscopy (TEM). TEM observations were conducted on a Philips CM 120 electron microscope at an acceleration voltage of 100 kV. Samples for TEM observations were prepared by placing 10 μL of micelle solutions at a concentration of 0.1 g/L on copper grids, which were successively coated with thin films of Formvar and carbon. No staining was required.

Stopped-Flow with Light-Scattering Detection. Stopped-flow studies were carried out using a Bio-Logic SFM300/S stopped-flow instrument. It is equipped with three 10 mL step-motor-driven syringes (S1, S2, and S3), which can be operated independently to carry out single or double mixing. The stopped-flow device is attached to a MOS-250 spectrometer; kinetic data were fitted using the Biokine program provided by Bio-Logic. For the light scattering detection at a scattering angle of 90°, both the excitation and emission wavelengths were adjusted to 335 nm with 10 nm slit widths. Using FC-08 or FC-15 flow cells, typical dead times are 1.1 and 2.6 ms, respectively.

Results and Discussion

Synthesis of PNIPAM$_{65}$-*b*-PBLG$_{110}$ and PNIPAM$_{65}$-*b*-PLGA$_{110}$. The general synthetic routes for the preparation of polypeptide hybrid diblock copolymers, PNIPAM-*b*-PBLG and PNIPAM-*b*-PLGA, were shown in Scheme 1.

Synthesis of PNIPAM$_{65}$-b-PBLG$_{110}$. Monoamino-terminated PNIPAM (PNIPAM-NH$_2$) was synthesized according to procedures reported by Chen et al.[52] via the free radical polymerization of NIPAM in methanol using AIBN and AET·HCl as the initiator and chain transfer agent, respectively. After further purification of the crude polydisperse PNIPAM-NH$_2$ by consecutive dialysis using semipermeable membranes with cutoff molar masses of 7000 and 14000 g/mol, respectively, PNIPAM fraction with relatively narrow polydispersity was collected. GPC analysis in THF reveals a monomodal and symmetric peak with an M_n of ~7400 and a polydispersity, M_w/M_n, of 1.31 (Figure S1, Supporting Information). The degree of polymerization, DP, of the final product was calculated to be ~65, and it was denoted as PNIPAM$_{65}$-NH$_2$.[29]

The terminal primary amine group of PNIPAM$_{65}$-NH$_2$ was then used as an initiating site for the ROP of BLG-NCA, leading to the formation of PNIPAM-*b*-PBLG diblock copolymer. The GPC trace clearly shows that the elution peak shifts to higher molecular weight after the ROP of BLG-NCA (Figure S1, Supporting Information), as compared to that of PNIPAM$_{65}$-NH$_2$ precursor. The elution peak of diblock copolymer is relatively symmetric and shows no discernible tailing at the lower molecular weight side, confirming a complete consumption of PNIPAM-NH$_2$. The molecular weight and molecular weight distribution of PNIPAM-*b*-PBLG were characterized by GPC analysis in THF: M_n = 35100, M_w/M_n = 1.29. The relatively narrow polydispersity of the obtained PNIPAM-*b*-PBLG could be explained by the living character of the ROP of NCAs initiated by primary amine residues. It should be noted that Cho et al.[24,55] also prepared PNIPAM-*b*-PBLG using similar procedures.

Figure S2 in Supporting Information shows ^{1}H NMR spectrum of PNIPAM-*b*-PBLG in $CDCl_3$ containing ~10 v/v% TFA, which can break up secondary aggregates or structures (e.g., α-helix) formed due to the association of polypeptide segments in nonpolar solvents.[56–58] It can be clearly seen that all signals characteristic of PNIPAM and PBLG blocks are visible. The signal at $\delta = 1.0$ ppm is ascribed to methyl protons (*a*) of the PNIPAM block; the resonance signals of protons on amide group (*g*), phenyl group (*h*), methylene group of benzyl (*f*), and methylene groups (*c*, *i*) of PBLG block occur at $\delta =$ 8.0–8.4, 7.1, 5.0, and 1.8–2.7 ppm, respectively. On the basis of the integral ratio of peaks *a* and *f*, the degree of polymerization, DP, of the PBLG block was calculated to be 110. Thus, the diblock copolymer was denoted as $PNIPAM_{65}$-*b*-$PBLG_{110}$.

Synthesis of $PNIPAM_{65}$-b-$PLGA_{110}$. The obtained $PNIPAM_{65}$-*b*-$PBLG_{110}$ was then subjected to hydrolysis to remove benzyl groups under alkaline conditions.[59,60] Figure S2 in Supporting Information also shows the ^{1}H NMR spectrum of the hydrolyzed product, $PNIPAM_{65}$-*b*-$PLGA_{110}$, in D_2O at pH 10. We can clearly see that signals characteristic of benzyl groups (peaks *h* and *f*) of PBLG block at 7.1 and 5.0 ppm completely disappear, indicating the complete removal of benzyl groups. It should be noted that the DP of PLGA blocks was also determined to be ~110 based on comparison of the integration areas of peaks *a* and *d*. This indicates that both the PNIPAM and the polyamide backbone of polypeptide blocks are unaffected during hydrolyzis.

Further verification of the complete removal of benzyl groups was established by FT-IR studies of $PNIPAM_{65}$-*b*-$PBLG_{110}$ and its hydrolyzed product, $PNIPAM_{65}$-*b*-$PLGA_{110}$ (Figure S3, Supporting Information). After deprotection, the characteristic absorption peaks of phenyl groups at 749 and 697 cm^{-1} completely disappeared. Meanwhile, the absorption peak at 1733 cm^{-1}, which is ascribed to the ester carbonyl of PBLG, was also absent. These results demonstrate that PNIPAM-*b*-PBLG diblock copolymer has been successfully converted to PNIPAM-*b*-PLGA, which is in general agreement with ^{1}H NMR results (Figure S2, Supporting Information).

"Schizophrenic" Micellization of PNIPAM-*b*-PLGA. It is well-known that PNIPAM homopolymer dissolves in cold and dilute aqueous solution but gets insoluble at ~32 °C due to its lower critical solution temperature (LCST) phase behavior.[50] On the other hand, poly(L-glutamic acid) takes a random coil conformation in aqueous solution at alkaline pH due to ionization of side carboxyl groups and an α-helix conformation in acidic media (the pK_a value of glutamic acid is 4.32).[61] Interestingly, pH-induced coil-to-helix transition is also accompanied by a considerable decrease of the water solubility of the PLGA block.[31] Thus, $PNIPAM_{65}$-*b*-$PLGA_{110}$ might exhibit thermo- and pH-responsive "schizophrenic" micellization behavior in aqueous solution, accompanied by coil-to-helix transitions (Scheme 2).

Thermo-Responsive Micellization of PNIPAM-b-PLGA. The $PNIPAM_{65}$-*b*-$PLGA_{110}$ diblock copolymer is directly soluble in alkaline water at 25 °C. Upon heating to 35 °C, a bluish tinge characteristic of micellar solutions appears. Figure 1 shows temperature-dependent optical transmittance obtained for 2.0 g/L aqueous solution of $PNIPAM_{65}$-*b*-$PLGA_{110}$ at pH 10. It can be clearly seen that the transmittance starts to decrease dramatically at ~30 °C, indicating that PNIPAM block is getting hydrophobic above its LCST. The transmittance stabilizes out above 45 °C, remaining almost constant at ~70%. This suggests complete thermo-induced micellization. On the basis of chemical

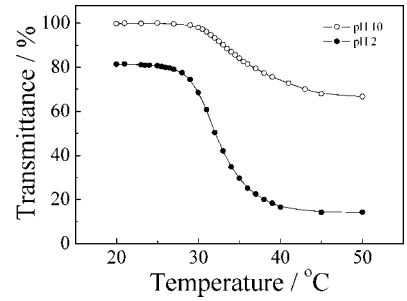

Figure 1. Temperature-dependent optical transmittance at 600 nm obtained for 2.0 g/L aqueous solution of $PNIPAM_{65}$-*b*-$PLGA_{110}$ at pH 10 and 2, respectively.

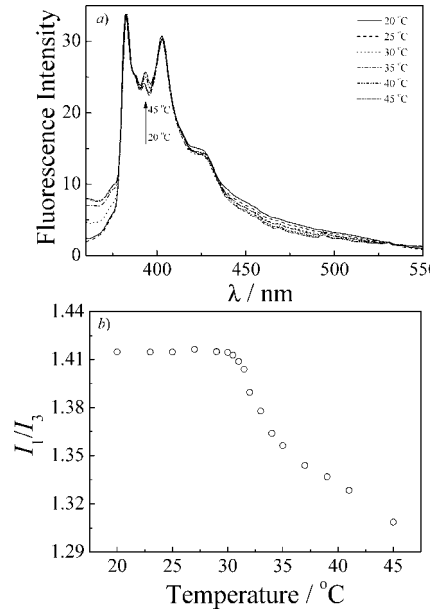

Figure 2. (a)Typical fluorescence emission spectra obtained for 2.0 g/L aqueous solution of $PNIPAM_{65}$-*b*-$PLGA_{110}$ at pH 10 and different temperatures; (b) plots of I_1/I_3 as a function of temperature. The polymer concentration was 2.0 g/L, and pyrene concentration was fixed at 5.0×10^{-7} mol/L.

intuition, the formed micelles should possess a core consisting of hydrophobic PNIPAM and a well-solvated PLGA corona (Scheme 2).

Information about the onset of the thermoresponsive micellization of $PNIPAM_{65}$-*b*-$PLGA_{110}$ at pH 10 can also be derived from steady-state fluorescence employing pyrene as a probe. Typical emission spectra obtained for aqueous solutions of $PNIPAM_{65}$-*b*-$PLGA_{110}$ (pH 10, 5.0×10^{-7} mol/L pyrene) at different temperatures are shown in Figure 2a. The emission spectra are characteristic of pyrene monomer fluorescence, where the ratio of the intensity of the first and third vibronic peaks, I_1/I_3, can be used to monitor the formation of hydrophobic microdomains. If micelles form at elevated temperatures, the hydrophobic PNIPAM core will tend to solubilize hydrophobic pyrene probes. A decrease in I_1/I_3 reflects the transfer of pyrene from a hydrophilic to a more hydrophobic microenvironment.

Apparently, we can observe a decrease of I_1/I_3 with increasing temperatures. Figure 2b shows the temperature dependence of I_1/I_3 ratios obtained for the aqueous solution of $PNIPAM_{65}$-*b*-$PLGA_{110}$ at pH 10. In the temperature range of 20–30 °C, I_1/I_3 ratios remain almost constant at ~1.42, indicating that the pyrene probe was located in a hydrophilic environment and extensive thermoresponsive micellization does not occur. Upon further increasing temperatures, I_1/I_3 values considerably decrease. The

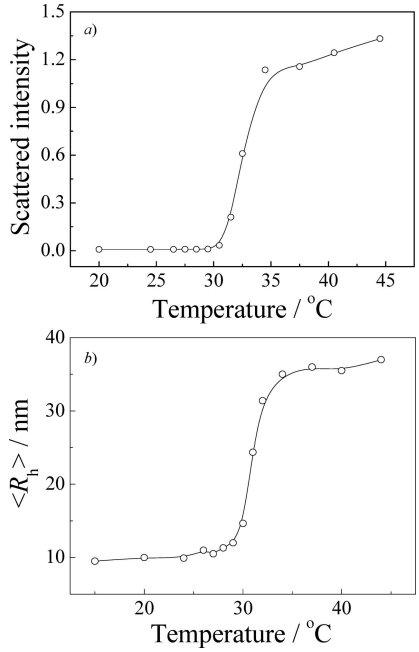

Figure 3. Variation of (a) intensity-average hydrodynamic radius, $\langle R_h \rangle$, and (b) scattered light intensity at a fixed scattering angle of 90 °C obtained for 1.0 g/L aqueous solution of $PNIPAM_{65}$-*b*-$PLGA_{110}$ at pH 10 as a function of temperature.

inflection point of the $I_1/I_3 \sim T$ curve at ~30.5 °C can thus be ascribed to the critical micellization temperature (CMT) of $PNIPAM_{65}$-*b*-$PLGA_{110}$ at pH 10 (Scheme 2). The CMT value obtained from fluorescence probe experiments generally agrees with that from optical transmittance results (Figure 1).

Dynamic LLS was then employed to characterize the thermo-induced formation of PNIPAM–core micelles. Figure 3 shows temperature dependence of scattered light intensity and average hydrodynamic radius, $\langle R_h \rangle$, obtained for an aqueous solution of $PNIPAM_{65}$-*b*-$PLGA_{110}$ at pH 10. Below 30 °C, the diblock copolymer molecularly dissolves with $\langle R_h \rangle$ of ca. 10 nm and very weak scattered light intensity. Above 30 °C, micellization starts to occur, as demonstrated by the dramatic increase of $\langle R_h \rangle$ and scattered intensity. At 35 °C, the measured intensity–intensity time correlation function and hydrodynamic radius distribution obtained by CONTIN analysis were shown in Figure S4 in Supporting Information, which reveal only one population corresponding to PNIPAM–core micelles with a polydispersity index, μ_2/Γ^2, of 0.11. $\langle R_h \rangle$ values remain almost constant at ~35 nm above 35 °C.

Figure 4 shows the scattering vector (q^2) dependence of the apparent diffusion coefficient, $\langle \Gamma \rangle / q^2$, obtained for $PNIPAM_{65}$-*b*-$PLGA_{110}$ aqueous solution at pH 10 and 45 °C. It can be clearly seen that $\langle \Gamma \rangle / q^2$ is almost independent of q^2 in the scattering angle range of 15°–90°. The weak angular dependences of $\langle \Gamma \rangle / q^2$ strongly suggest that PNIPAM–core micelles should take spherical shapes. The morphology of PNIPAM–core micelles has been further confirmed by TEM observation (Figure 5a), which reveals the presence of nearly spherical nanoparticles.

Static LLS measurement of PNIPAM–core micellar solution at a concentration of 0.05 g/L (pH 10, 45 °C) yielded an apparent micelle molar mass, $M_{w,app}$, of 1.53×10^7 g/mol. The average aggregation number, N_{agg}, of diblock copolymer chains inside each micellar aggregate was then calculated to be ~590.

The thermoresponsive micellization behavior of $PNIPAM_{65}$-*b*-$PLGA_{110}$ was further investigated by ^{1}H NMR spectra, which can conveniently reveal which block sequence in the copolymer

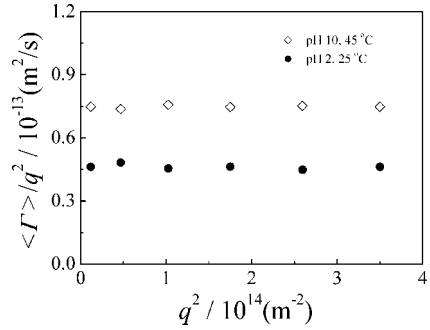

Figure 4. Scattering vector (q^2) dependence of the apparent translational diffusion coefficient $\langle \Gamma \rangle / q^2$ obtained for 1.0 g/L aqueous solution of $PNIPAM_{65}$-*b*-$PLGA_{110}$ at pH 10 and 45 °C (□), and pH 2 and 25 °C (●), respectively.

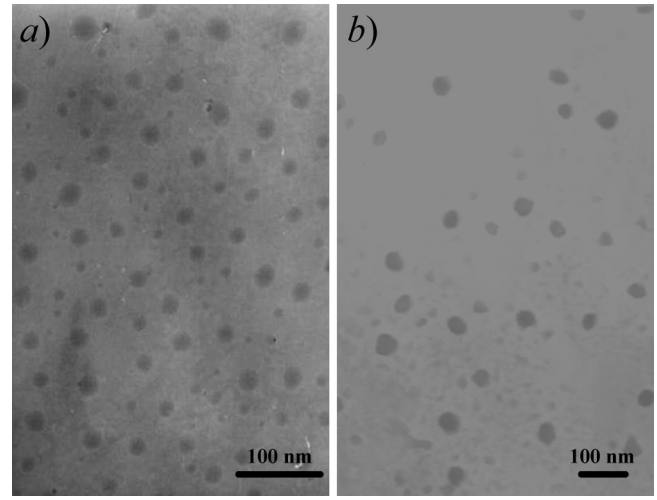

Figure 5. TEM images of PNIPAM–core and PLGA–core micelles formed from $PNIPAM_{65}$-*b*-$PLGA_{110}$ at (a) pH 10 and 45 °C and (b) pH 2 and 25 °C, respectively.

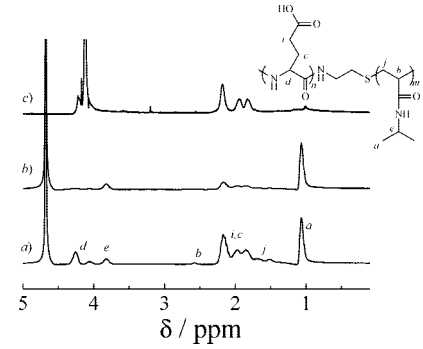

Figure 6. ^{1}H NMR spectra of $PNIPAM_{65}$-*b*-$PLGA_{110}$ in D_2O at (a) pH 10 and 25 °C, (b) pH 2 and 25 °C, and (c) pH 10 and 45 °C.

is forming the micelle core.[62–64] At pH 10 and 25 °C, $PNIPAM_{65}$-*b*-$PLGA_{110}$ is fully solvated, thus characteristic signals of both blocks are visible (Figure 6a). Upon heating to 45 °C, ^{1}H NMR spectrum clearly reveals that the relative intensity of characteristic PLGA signals at 1.8–2.3 ppm remains unchanged, whereas the characteristic PNIPAM resonance signal at 1.0 ppm nearly disappears (Figure 6c). This further supports the formation of PNIPAM–core micelles stabilized by ionized PLGA coronas at elevated temperatures and pH 10 (Scheme 2). It should be noted that the PLGA block in the micelle corona takes a random coil conformation in alkaline conditions.[61]

pH-Responsive Micellization of PNIPAM-b-PLGA. Starting from the unimer state of $PNIPAM_{65}$-*b*-$PLGA_{110}$ in aqueo

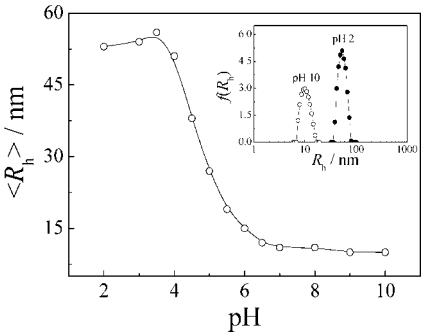

Figure 7. Variation of intensity-average hydrodynamic radius, $\langle R_h \rangle$, obtained for 1.0 g/L aqueous solution of $PNIPAM_{65}$-*b*-$PLGA_{110}$ at 25 °C as a function of pH. The inset shows typical hydrodynamic radius distributions, $f(R_h)$, at pH 10 (○) and 2 (●), respectively.

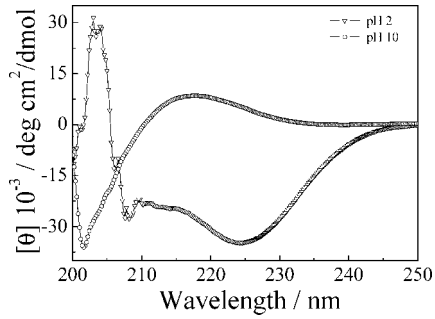

Figure 8. Circular dichroism spectra obtained for 0.2 g/L aqueous solution of $PNIPAM_{65}$-*b*-$PLGA_{110}$ at 25 °C and different pH values.

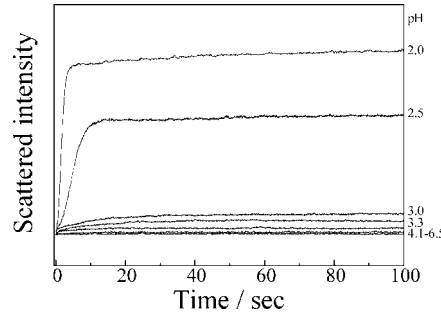

Figure 9. Time dependence of scattered light intensity recorded for aqueous solutions of $PNIPAM_{65}$-*b*-$PLGA_{110}$ upon a pH jump from 10 to various final pH values. The final polymer concentrations were fixed at 1.0 g/L.

solution at pH 10 and 25 °C, PLGA–core micelles can also be fabricated via pH changes (Scheme 2). Upon addition of a small amount of concentrated HCl solution, a bluish tinge characteristic of micellar solutions also appears. The pH-induced micellization behavior of $PNIPAM_{65}$-*b*-$PLGA_{110}$ aqueous solution was studied by means of ^{1}H NMR, optical transmittance, TEM, dynamic and static LLS, and CD spectroscopy.

At pH 2 and 25 °C, ^{1}H NMR resonance signals characteristic of PLGA block at 4.0–4.3 and 1.8–2.3 ppm almost completely disappear, indicating that PLGA block gets insoluble at acidic pH (Figure 6b); on the other hand, resonance signals characteristic of PNIPAM segments are still clearly evident. These results suggest the formation of structurally "inverted" PLGA–core micelles stabilized with PNIPAM coronas (Scheme 2).

The pH-induced PLGA–core micelles were further characterized by dynamic LLS. Figure 7 shows the pH dependence of $\langle R_h \rangle$ for aqueous solution (25 °C) of $PNIPAM_{65}$-*b*-$PLGA_{110}$. At pH 10, the diblock copolymer is molecularly soluble and the aqueous solution is clear, exhibiting $\langle R_h \rangle$ of ~10 nm. Below pH 6, $\langle R_h \rangle$ increases dramatically, indicating that micellization starts to occur. At pH 2, $\langle R_h \rangle$ of PLGA–core micelles is ~53 nm and the polydispersity index, μ_2/Γ^2, is 0.15. The inset of Figure 6 shows that the hydrodynamic radius distribution curve shifts to higher values upon decreasing from pH 10 to 2, clearly confirming the formation PLGA–core micelles.

The actual morphology of the PLGA–core micelles can be directly obtained by TEM observation (Figure 5b), which clearly reveals the presence of spherical micelles with an average diameter of ~40 nm. This result is in general agreement with the weak q^2 dependence of $\langle \Gamma \rangle / q^2$ obtained for aqueous solution of $PNIPAM_{65}$-*b*-$PLGA_{110}$ at pH 2 and 25 °C (Figure 4). Lecommandoux et al.[31] synthesized $PLGA_{15}$-*b*-PLL_{15} diblock copolymer. At pH 3 and 12, this intriguing polypeptide-based copolymer self-assembled into two types of vesicles with invertible microstructures. In the current case, polypeptide hybrid diblock copolymer $PNIPAM_{65}$-*b*-$PLGA_{110}$ forms spherical PNIPAM–core and PLGA–core micelles at two different solution conditions (Scheme 2).

Static LLS measurement of PLGA–core micellar solution at a concentration of 0.05 g/L (pH 2, 25 °C) yielded an apparent micelle molar mass, $M_{w,app}$, of 7.28×10^7 g/mol. The average aggregation number, N_{agg}, of diblock copolymer chains of PLGA–core micelles was then calculated to be ~2800. The much larger N_{agg} of PLGA–core micelles compared to that of PNIPAM–core micelles should be due to the much longer PLGA block relative to that of PNIPAM sequence. The size of PLGA–core micelles is very large considering the chemical structure of $PNIPAM_{65}$-*b*-$PLGA_{110}$. If all polymer chains are in a stretched conformation, the diameter of the micelles in solution should not exceed $175 \times 2 \times 0.25$ nm = 87.5 nm. Thus some PNIPAM blocks must be located within the PLGA cores. We thus tentatively ascribe the formation of large hybrid nanoparticles to large compound micelles (LCM).[65]

Figure 1 also shows the temperature-dependent optical transmittance obtained for $PNIPAM_{65}$-*b*-$PLGA_{110}$ aqueous solution at pH 2. At 20 °C, a bluish tinge characteristic of micellar solutions appears, with an optical transmittance of ~80% at 600 nm wavelength. Above 28 °C, the transmittance starts to decrease dramatically to ~15% at 50 °C, which could be attributed to thermal phase transitions of PNIPAM coronas and subsequent intermicellar aggregation, leading to macroscopic phase separations.

It is well-known that upon pH decrease, the PLGA sequence also exhibits the secondary conformational transition from a charged coil to a more compact α-helical structure at acidic pH.[39,41,42,66] CD spectroscopy was then employed to investigate the pH-dependent conformational transitions of PLGA sequences accompanied with the pH-induced formation of PLGA–core micelles (Figure 8). The CD spectrum of $PNIPAM_{65}$-*b*-$PLGA_{110}$ in aqueous solution at pH 10 is characteristic of random coil conformations. Under acidic conditions (pH 2), two negative bands at 208 and 224 nm can be detected, which can be assigned to π–π^* and n–π^* transitions, respectively, due to Cotton effects. These features are characteristic of α-helix secondary structures. From the absolute value of molar ellipticity, θ, at a wavelength of 208 nm, we can estimate that the percentage of α-helix conformations is 0% at pH 10 and ~80% at pH 2.[61,67]

Kinetics of pH-Induced Formation of PLGA–Core Micelles. Figure 9 shows the time dependence of scattered light intensity upon a pH jump from 10 to various final pH values. If the final pH is above 4.1, the kinetic trace remains a straight line. The diblock copolymer chains exist as unimers, and we do not observe any relaxation processes. Upon a pH jump fro

10 to the final pH range of 3.0–3.3, scattered light intensity gradually increases and then stabilizes out after ~30–40 s. At a final pH range of 2.0–2.5, scattered light intensity shows an abrupt increase within the initial 5–10 s and then reaches the final plateau value. Apparently, we can tell that the lower final pH values, the faster the pH-induced micelle growth. Figure 9 also reveals that at lower final pH, the formed PLGA–core micelles possess larger aggregation numbers per micelle, N_{agg}, as revealed by the larger equilibrium scattered values.

Previously, we investigated the pH-induced micellization kinetics of poly(4-vinylbenzoic acid)-*b*-poly(*N*-(morpholino)ethyl methacrylate) (PVBA-*b*-PMEMA).[68] The PVBA block is insoluble at low pH and soluble in alkaline media. Although the PVBA chains within micelle cores at low pH can also interact via intra- or intermolecular hydrogen bonding interactions due to the presence of protonated carboxyl groups, the pH-induced micellization takes a considerably long time. Semenov et al.[69,70] recently postulated that the unimer-to-micelle transition can be characterized by a continuous spectrum of relaxation times, and the main route to micelle formation should involve step-by-step addition of unimers, i.e., the insertion/expulsion of individual chains.[69] They also suggested that the growing micelles will never reach the near-equilibrium size and their growth might be arrested at an intermediate stage.

The pH-induced micellization of PNIPAM-*b*-PLGA exhibits drastically different kinetics compared to that of PVBA-*b*-PMEMA (Figure 9).[68] If the final pH is ≤2.5, the scattered light intensity quickly stabilizes out after the initial fast increase. This might be ascribed to the formation of α-helix secondary structures within PLGA cores, which provides additional stabilization effects for the formed micelles. We can reasonably expect that these α-helix secondary structures can greatly restrict elementary steps associated with micelle formation/breakup, i.e., unimer insertion/expulsion or micelle fusion/fission. It should be noted that currently there is a lack of related theory concerning the kinetics of unimer-to-micelle transitions that is accompanied by the formation of secondary structures.

Conclusion

The pH- and thermoresponsive "schizophrenic" micellization behavior of a polypeptide hybrid double hydrophilic diblock copolymer, $PNIPAM_{65}$-*b*-$PLGA_{110}$, was thoroughly investigated via a combination of ^{1}H NMR, optical transmittance, fluorescence probe measurement, transmission electron microscopy (TEM), dynamic and static laser light scattering (LLS), and circular dichroism (CD) spectroscopy. $PNIPAM_{65}$-*b*-$PLGA_{110}$ supramolecularly self-assembles into PNIPAM–core micelles at alkaline pH and elevated temperatures and PLGA–core micelles at acidic pH and room temperature. "Schizophrenic" micellization of $PNIPAM_{65}$-*b*-$PLGA_{110}$ leads to the facile locating of peptide sequence either within micelle cores or stabilizing coronas. Moreover, stopped-flow studies reveal that the formation of α-helix secondary structures at low pH exerts considerable effects on the pH-induced micellization kinetics of $PNIPAM_{65}$-*b*-$PLGA_{110}$. The incorporation of polypeptide sequences into DHBCs can endow them with structural versatility, tunable spatial arrangement of chain segments within self-assembled nanostructures, enhanced biocompatibility, and broader applications in the field of biomedicines, which might represent a promising new direction in the field of DHBCs within the context of both academic studies and practical applications.

Acknowledgment. This work was financially supported by an Outstanding Youth Fund (50425310) and research grants (20534020 and 20674079) from the National Natural Scientific Foundation of China (NNSFC), the "Bai Ren" Project and Special Grant (KJCX2-SW-H14) of the Chinese Academy of Sciences, and the Program for Changjiang Scholars and Innovative Research Team in University (PCSIRT).

Supporting Information Available. Detailed experimental procedures, ^{1}H NMR, GPC, FT-IR characterization results, and dynamic LLS characterization details. This information is available free of charge via the Internet at http://pubs.acs.org.

References and Notes

(1) Moffitt, M.; Khougaz, K.; Eisenberg, A. *Acc. Chem. Res.* **1996**, *29*, 95–102.
(2) Liu, G. J.; Qiao, L. J.; Guo, A. *Macromolecules* **1996**, *29*, 5508–5510.
(3) Gohy, J. F.; Creutz, S.; Garcia, M.; Mahltig, B.; Stamm, M.; Jerome, R. *Macromolecules* **2000**, *33*, 6378–6387.
(4) Zhang, L. F.; Eisenberg, A. *J. Am. Chem. Soc.* **1996**, *118*, 3168–3181.
(5) Zhang, L. F.; Eisenberg, A. *Science* **1995**, *268*, 1728–1731.
(6) Discher, B. M.; Won, Y. Y.; Ege, D. S.; Lee, J. C. M.; Bates, F. S.; Discher, D. E.; Hammer, D. A. *Science* **1999**, *284*, 1143–1146.
(7) Cornelissen, J. J.; Fischer, M.; Sommerdijk, N. A.; Nolte, R. J. *Science* **1998**, *280*, 1427–1430.
(8) Yu, G. E.; Eisenberg, A. *Macromolecules* **1998**, *31*, 5546–5549.
(9) Schlaad, H.; Antonietti, M. *Eur. Phys. J. E* **2003**, *10*, 17–23.
(10) Gallot, B. *Prog. Polym. Sci.* **1996**, *21*, 1035–1088.
(11) Vandermeulen, G. W. M.; Klok, H. A. *Macromol. Biosci.* **2004**, *4*, 383–398.
(12) Klok, H. A. *J. Polym. Sci., Part A: Polym. Chem.* **2005**, *43*, 1–17.
(13) Klok, H. A.; Lecommandoux, S. *Adv. Polym. Sci.* **2006**, *202*, 75–111.
(14) Deming, T. J. *Adv. Polym. Sci.* **2006**, *202*, 1–18.
(15) Schlaad, H. *Adv. Polym. Sci.* **2006**, *202*, 53–73.
(16) Klok, H. A.; Langenwalter, J. F.; Lecommandoux, S. *Macromolecules* **2000**, *33*, 7819–7826.
(17) Crespo, J. S.; Lecommandoux, S.; Borsali, R.; Klok, H. A.; Soldi, V. *Macromolecules* **2003**, *36*, 1253–1256.
(18) Checot, F.; Lecommandoux, S.; Klok, H. A.; Gnanou, Y. *Eur. Phys. J. E* **2003**, *10*, 25–35.
(19) Checot, F.; Lecommandoux, S.; Gnanou, Y.; Klok, H. A. *Angew. Chem., Int. Ed.* **2002**, *41*, 1339–1343.
(20) Checot, F.; Brulet, A.; Oberdisse, J.; Gnanou, Y.; Mondain-Monval, O.; Lecommandoux, S. *Langmuir* **2005**, *21*, 4308–4315.
(21) Lubbert, A.; Castelletto, V.; Hamley, I. W.; Nuhn, H.; Scholl, M.; Bourdillon, L.; Wandrey, C.; Klok, H. A. *Langmuir* **2005**, *21*, 6582–6589.
(22) Cho, C. S.; Kwon, J. K. *Korea Polym. J.* **1999**, *7*, 208–212.
(23) Cho, C. S.; Jo, B. W.; Kwon, J. K.; Komoto, T. *Macromol. Chem. Phys.* **1994**, *195*, 2195–2206.
(24) Cho, C. S.; Cheon, J. B.; Jeong, Y. I.; Kim, I. S.; Kim, S. H.; Akaike, T. *Macromol. Rapid Commun.* **1997**, *18*, 361–369.
(25) Chung, T. W.; Kim, B. J.; Park, S. Y.; Akaike, T.; Nah, J. W.; Cho, C. S. *Macromolecules* **2000**, *33*, 8921–8923.
(26) Yoo, M. K.; Jang, M. K.; Nah, J. W.; Park, M. R.; Cho, C. S. *Macromol. Chem. Phys.* **2006**, *207*, 528–535.
(27) Zhu, Z. Y.; Armes, S. P.; Liu, S. Y. *Macromolecules* **2005**, *38*, 9803–9812.
(28) Xu, J.; Ge, Z. S.; Zhu, Z. Y.; Luo, S. Z.; Liu, H. W.; Liu, S. Y. *Macromolecules* **2006**, *39*, 8178–8185.
(29) Ge, Z. S.; Cai, Y. L.; Yin, J.; Zhu, Z. Y.; Rao, J. Y.; Liu, S. Y. *Langmuir* **2007**, *23*, 1114–1122.
(30) Colfen, H. *Macromol. Rapid Commun.* **2001**, *22*, 219–252.
(31) Rodriguez-Hernandez, J.; Lecommandoux, S. *J. Am. Chem. Soc.* **2005**, *127*, 2026–2027.
(32) Andre, X.; Zhang, M. F.; Muller, A. H. E. *Macromol. Rapid Commun.* **2005**, *26*, 558–563.
(33) Schilli, C. M.; Zhang, M. F.; Rizzardo, E.; Thang, S. H.; Chong, Y. K.; Edwards, K.; Karlsson, G.; Muller, A. H. E. *Macromolecules* **2004**, *37*, 7861–7866.
(34) Gil, E. S.; Hudson, S. A. *Prog. Polym. Sci.* **2004**, *29*, 1173–1222.
(35) Gan, L. H.; Ravi, P.; Mao, B. W.; Tam, K. C. *J. Polym. Sci., Part A: Polym. Chem.* **2003**, *41*, 2688–2695.
(36) Butun, V.; Liu, S.; Weaver, J. V. M.; Bories-Azeau, X.; Cai, Y.; Armes, S. P. *React. Funct. Polym.* **2006**, *66*, 157–165.
(37) Gohy, J. F. *Adv. Polym. Sci.* **2005**, *190*, 65–136.

(38) Riess, G. *Prog. Polym. Sci.* **2003**, *28*, 1107–1170.
(39) Adler, A. J.; Hoving, R.; Potter, J.; Wells, M.; Fasman, G. D. *J. Am. Chem. Soc.* **1968**, *90*, 4736–4738.
(40) Dai, Q. Y.; Prorok, M.; Castellino, F. J. *J. Mol. Biol.* **2004**, *336*, 731–744.
(41) Ernst, J. T.; Kutzki, O.; Debnath, A. K.; Jiang, S.; Lu, H.; Hamilton, A. D. *Angew. Chem., Int. Ed.* **2001**, *41*, 278–281.
(42) Spek, E. J.; Gong, Y. X.; Kallenbach, N. R. *J. Am. Chem. Soc.* **1995**, *117*, 10773–10774.
(43) Davidson, B.; Fasman, G. D. *Biochemistry* **1967**, *6*, 1616–1629.
(44) Mathews, D. H.; Turner, D. H. *Biochemistry* **2002**, *41*, 869–880.
(45) Morawetz, H.; Cho, J. R.; Gans, P. J. *Macromolecules* **1973**, *6*, 624–627.
(46) Muller, M.; Buchet, R.; Fringeli, U. P. *J. Phys. Chem.* **1996**, *100*, 10810–10825.
(47) Yaworsky, D. C.; Baker, B. Y.; Bose, H. S.; Best, K. B.; Jensen, L. B.; Bell, J. D.; Baldwin, M. A.; Miller, W. L. *J. Biol. Chem.* **2005**, *280*, 2045–2054.
(48) Meyer, M.; Schlaad, H. *Macromolecules* **2006**, *39*, 3967–3970.
(49) Agut, W.; Taton, D.; Lecommandoux, S. *Macromolecules* **2007**, *40*, 5653–5661.
(50) Schild, H. G. *Prog. Polym. Sci.* **1992**, *17*, 163–249.
(51) Blout, E. R.; Karlson, R. H. *J. Am. Chem. Soc.* **1956**, *78*, 941–946.
(52) Chen, G. H.; Hoffman, A. S. *Nature* **1995**, *373*, 49–52.
(53) Zhang, J. X.; Qiu, L. Y.; Zhu, K. J.; Yin, Y. *Macromol. Rapid Commun.* **2004**, *25*, 1563–1567.
(54) Durand, A.; Hourdet, D. *Polymer* **1999**, *40*, 4941–4951.
(55) Cheon, J. B.; Jeong, Y. I.; Cho, C. S. *Polymer* **1999**, *40*, 2041–2050.
(56) Bovey, F. A.; Ryan, J. J.; Spach, G.; Heitz, F. *Macromolecules* **1971**, *4*, 433–434.
(57) Bradbury, E. M.; Cary, P. D.; Crane-Robinson, C. *Macromolecules* **1972**, *5*, 581–589.
(58) Ferretti, J. A.; Ninham, B. W. *Macromolecules* **1970**, *3*, 30–33.
(59) Kaneko, T.; Asoh, T.; Fukushige, Y.; Akashi, M. *Macromolecules* **2006**, *39*, 2298–2305.
(60) Rodriguez-Hernandez, J.; Babin, J.; Zappone, B.; Lecommandoux, S. *Biomacromolecules* **2005**, *6*, 2213–2220.
(61) Kukula, H.; Schlaad, H.; Antonietti, M.; Forster, S. *J. Am. Chem. Soc.* **2002**, *124*, 1658–1663.
(62) Vamvakaki, M.; Palioura, D.; Spyros, A.; Armes, S. P.; Anastasiadis, S. H. *Macromolecules* **2006**, *39*, 5106–5112.
(63) Forder, C.; Patrickios, C. S.; Armes, S. P.; Billingham, N. C. *Macromolecules* **1996**, *29*, 8160–8169.
(64) Cau, F.; Lacelle, S. *Macromolecules* **1996**, *29*, 170–178.
(65) Cameron, N. S.; Corbierre, M. K.; Eisenberg, A. *Can. J. Chem.* **1999**, *77*, 1311.
(66) Appel, P.; Yang, J. T. *Biochemistry* **1965**, *4*, 1244–1249.
(67) Greenfield, N. J.; Fasman, G. D. *Biochemistry* **1969**, *8*, 4108–4116.
(68) Wang, D.; Yin, J.; Zhu, Z. Y.; Ge, Z. S.; Liu, H. W.; Armes, S. P.; Liu, S. Y. *Macromolecules* **2006**, *39*, 7378–7385.
(69) Nyrkova, I. A.; Semenov, A. N. *Macromol. Theory Simul.* **2005**, *14*, 569–585.
(70) Nyrkova, I. A.; Semenov, A. N. *Faraday Discuss.* **2005**, *128*, 113–127.

BM700830B